Supporting Information

Controlled Synthesis of Hollow Micro/Meso-Pore Nitrogen-Doped Carbon with Tunable Wall Thickness and Specific Surface Area as Efficient Electrocatalysts for Oxygen Reduction Reaction

Rui Wu, Siguo Chen,* Yuanliang Zhang, Yao Wang, Yao Nie, Wei Ding, Xueqiang Qi, and Zidong Wei*

Chongqing Key Laboratory of Chemical Process for Clean Energy and Resource Utilization, School of Chemistry and Chemical Engineering, Chongqing University, Shazhengjie 174, Chongqing 400044, China

Experimental

Synthesis of Silica spheres: Silica spheres employed as templates were synthesized by Stöber method. [1] Tetraethylorthosilicate (10 mL) in ethanol (60 mL) was added to a mixture of ammonia solution (28~30%, 8 mL), ethanol (150 mL) and deionized water (20 mL). The mixture was stirred for 4 hours. The produced silica spheres were isolated by centrifugation, washed with ethanol and dried under vacuum for 12 hours.

Synthesis of Hollow micro/meso-pore nitrogen-doped carbon (HMNC): 100 mg silica spheres were dispersed in the solution mixtures of deionized water (10 mL) and ethanol (10 mL). The dopamine (200 mg) in Tris-HCl (30 mL, 50 mM, pH≈8.5) solution was added. The reaction mixture was stirred for 24 hours at room temperature. The obtained polydopamine/silica (SiO_2@PDA) nanocomposite was collected by centrifugation and washed with deionized water and then dried at 60 ℃ for 12 h. After that, the SiO_2@PDA was stirred with $FeCl_3$ in deionized water to coordinate Fe (III) ions with -OH in PDA structure. The SiO_2@MNC composites were obtained by pyrolysis of SiO_2@PDA-Fe under N_2 atmosphere for 2h at preferable temperatures. The SiO_2@MNC was added to HF solution (5%, 20 mL) and the reaction mixture was stirred for 12 hours. The HMNC were retrieved by centrifugation, washed with water, ethanol, and dried at 60 ℃ for 12 hours.

Typical sample notation is as follows: HMNC-X-T, where X represents the weight ratio between the Fe (III) ions and the SiO_2@PDA (X= 0, 0.2, 0.5, 0.8 and 1.0) and T stands for the temperature (℃) of carbonization (T= 700, 800 and 900℃).

Electrochemical measurements: All electrochemical experiments were performed in a standard three-electrode cell at room temperature. The cell consisted of a glassy carbon working electrode (GC electrode, 5 mm in diameter, PINE: AFE3T050GC), an Ag/AgCl (saturated KCl) reference electrode, and a platinum foil counter electrode. All potentials in this study, however, are given relative to a reversible hydrogen electrode (RHE). The working electrodes were prepared by applying catalyst ink onto glassy carbon (GC) disk electrodes. In brief, the electrocatalyst was dispersed in ethanol and ultrasonicated for 30 minutes to form a uniform catalyst ink (10 μg μL^{-1}). A total of 10 μL of catalyst ink was then pipetted on the glassy carbon surface, leading to a loading of 0.5 mg cm^{-2}.

After drying at room temperature, a drop of 0.01wt% Nafion solution (Dupont) was applied onto the surface of the catalyst layer to form a thin protective film. The prepared electrodes were dried at room temperature before the electrochemical tests. All of the electrodes were pretreated by cycling the potential between 0 and 1.2 V at a sweep rate of 50 mV s^{-1} for 50 cycles in order to remove any surface contamination prior to ORR activity testing.

The activities of catalysts were performed by recording linear sweep voltammetry (LSV) curves in the oxygen-saturated 0.1 M KOH or 0.1 M $HClO_4$ solution. The LSV curves for ORR were recorded at potential scan rate of 10 mV s^{-1}. The rotation speed was controlled at 1,600 rpm.

Rotating disk electrode (RDE) measurements were conducted at rotation speeds from 100 to 2,500 rpm using a VersaSTAT3 (V_3). RDE measurements were conducted in O_2-saturated 0.1 M KOH solution at 10 mV s^{-1} scan rate. The electron transfer number (n)

was analyzed on the basis of Koutecky-Levich equations shown in equations.

$$\frac{1}{J} = \frac{1}{J_D} + \frac{1}{J_K} = \frac{1}{B\omega^{1/2}} + \frac{1}{J_K} \quad (1)$$

$$B = 0.62nFC_0(D_0)^{2/3}\upsilon^{-1/6} \quad (2)$$

in which J is the measured current density, J_K and J_D are the kinetic- and diffusion-limiting current densities, ω is the angular velocity of the disk ($\omega = 2\pi N$, N is the linear rotation speed), n is the overall number of electrons transferred in ORR, F is the Faraday constant (F=96,485 C mol^{-1}), C_0 is the bulk concentration of O_2, υ is the kinematic viscosity of the electrolyte, and k is the electron transfer rate constant. According to Equations (1) and (2), the number of electrons transferred (n) and J_K can be obtained from the slope and intercept of the Koutecky–Levich plots, respectively. By using the value C_0=1.2×10^{-3} mol L^{-1}, D_0=1.9×10^{-5} cm s^{-1} and υ=0.1 m^2 s^{-1} in 0.1M KOH

The CV accelerating stress tests (AST) were performed at potentials between 0 and 1.2 V versus a reversible hydrogen electrode (RHE) at a scan rate of 50 mV s^{-1} in nitrogen-purged 0.1 M KOH at room temperature. RDE cycling stability tests of the catalysts were performed in N_2-saturated 0.1 M KOH in the potential range of 0 to 1.2 V vs. RHE.

Electrochemical impedance spectroscopy (EIS) measurements were recorded in O_2-saturated 0.1 M KOH at 0.85 V vs. RHE with 10 mV ac potential from 10 kHz to 0.01 Hz. The loading was 0.5 mg cm^{-2} for all materials. Electrode rotation speed, 1,600 rpm.

Characterization

TEM test: Transmission electron microscopy (TEM) was carried out on a Zeiss LIBRA 200 FETEM instrument operating at 200 kV.

SEM test: Scanning electron microscope (SEM) was obtained using a JSM-7800F (JEOL) field emission scanning electron microscope operated at an acceleration voltage of 15 kV.

Raman spectrum test: Raman spectrum was recorded by a LabRamHR evolution Raman spectrometer equipped with a Nb-Yag laser excitation source operating at 532 nm.

XPS test: X-ray Photoelectron Spectroscopy (XPS) was conducted on a PE PHI-5400 spectrometer equipped with a monochromatic Al X-ray source (Al KR, 1.4866 keV). High-resolution elemental analysis was performed on the C 1s (295–275 eV), N 1s (390–410 eV) regions with a pass energy of 20 eV, a step of 0.05 eV, and an 800 ms dwell time. Each spectrum was constructed from an average of two scans. The pressure in the XPS analysis chamber was maintained at 10^{-7} Pa or lower during collection. In the data analysis, the binding energy (BE) of the core level C 1s peak was set at 284.5 eV to compensate for surface-charging effects. The Shirley background was subtracted, and the satellite peaks were removed for all element peaks before curve fitting. The experimental spectra were fitted into a Gaussian line shape. The surface elemental compositions were determined by the ratios of peak areas that had been corrected with empirical sensitivity factors

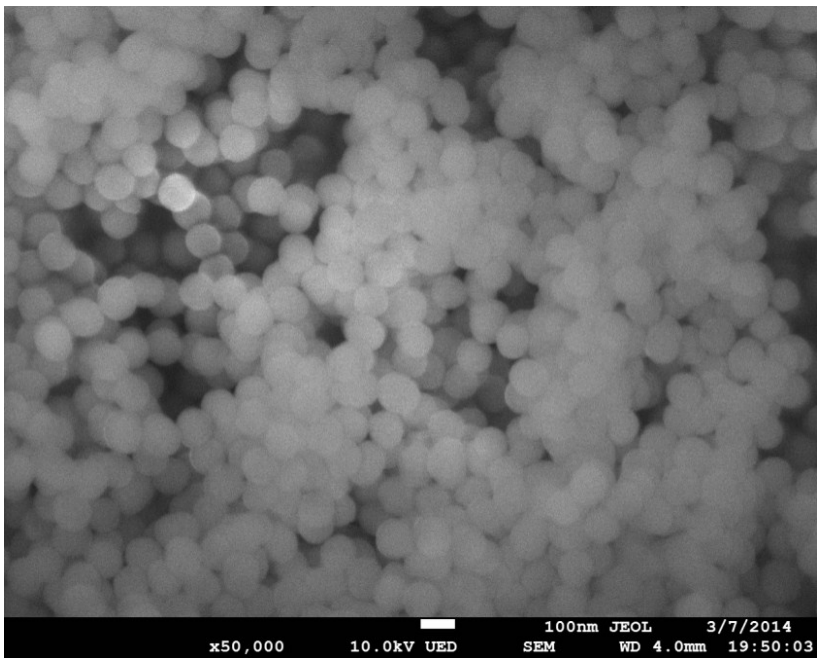

Figure S1. SEM image of silica spheres.

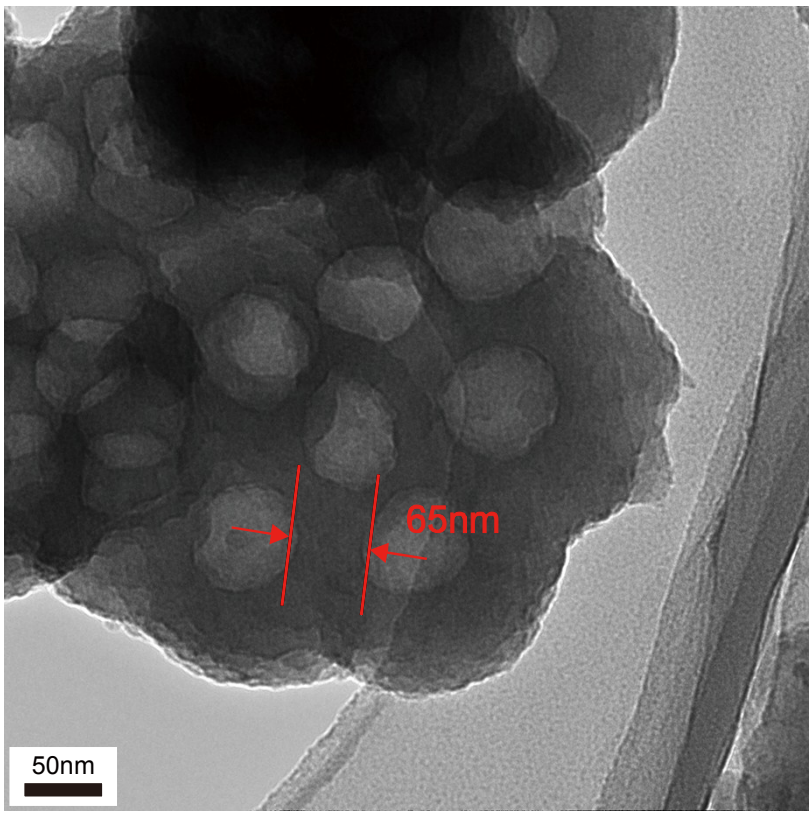

Figure S2. TEM image of hollow PDA.

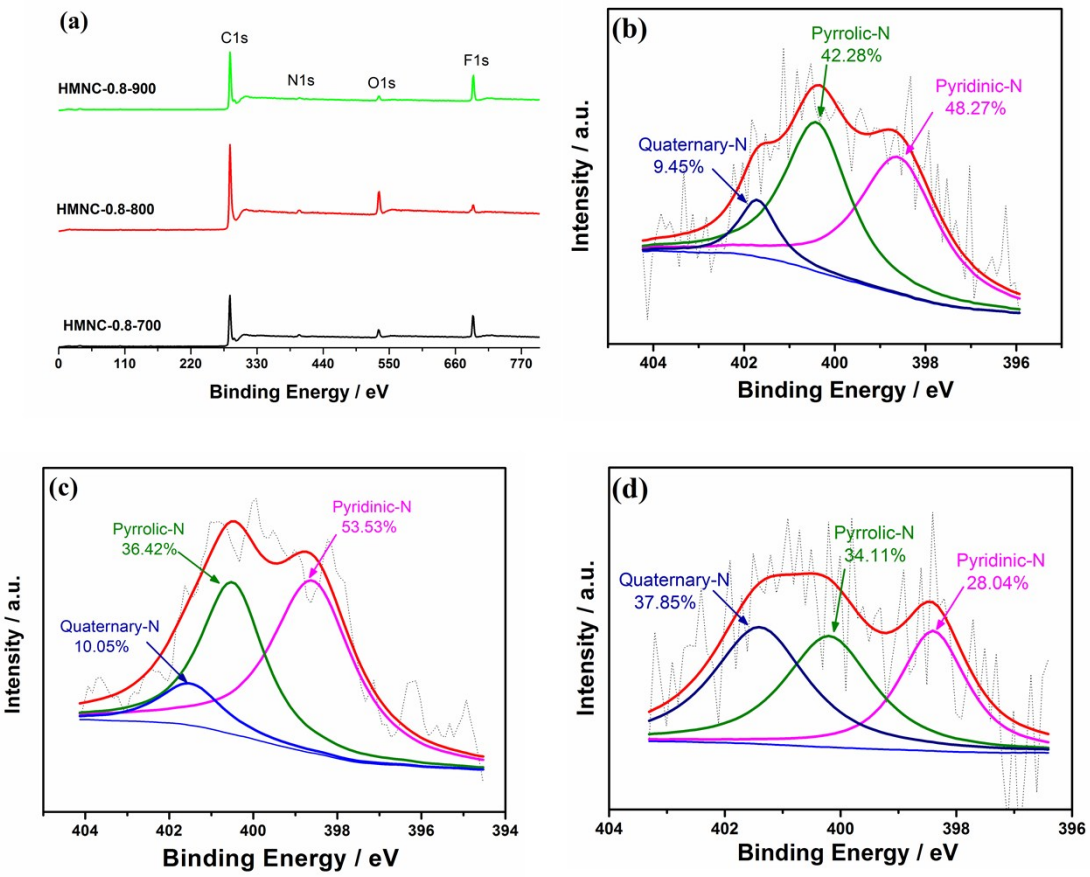

Figure S3. (a) XPS survey spectrum of HMNC-0.8-700, HMNC-0.8-800 and HMNC-0.8-900. XPS spectra of N 1s (b) HMNC-0.8-700, (c) HMNC-0.8-800, (d) HMNC-0.8-900.

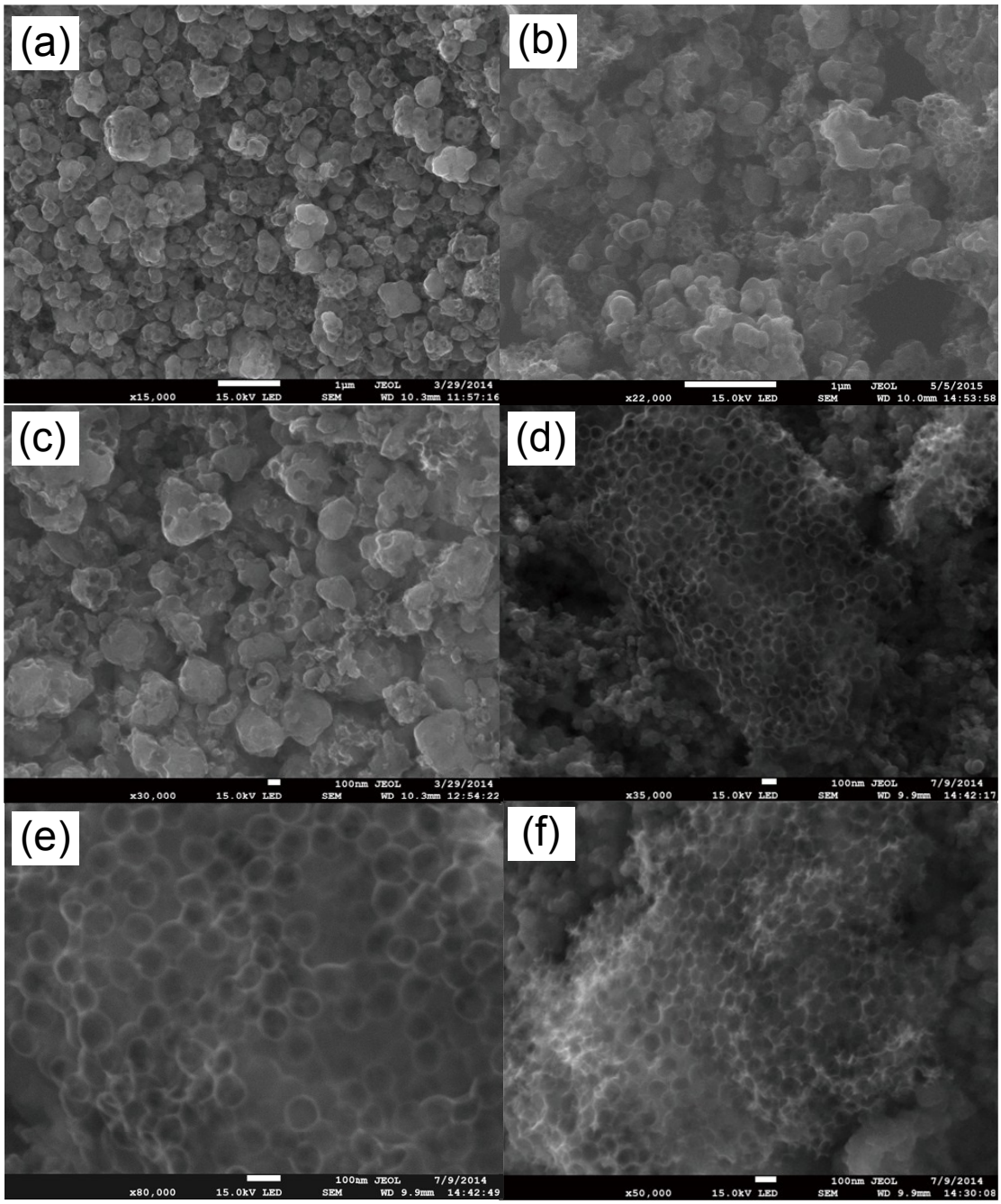

Figure S4. SEM images of (a) HMNC-0-800, (b) HMNC-0.2-800, (c) MNC-0.5-800, (d-e) HMNC-0.8-800, and (f) HMNC-1-800.

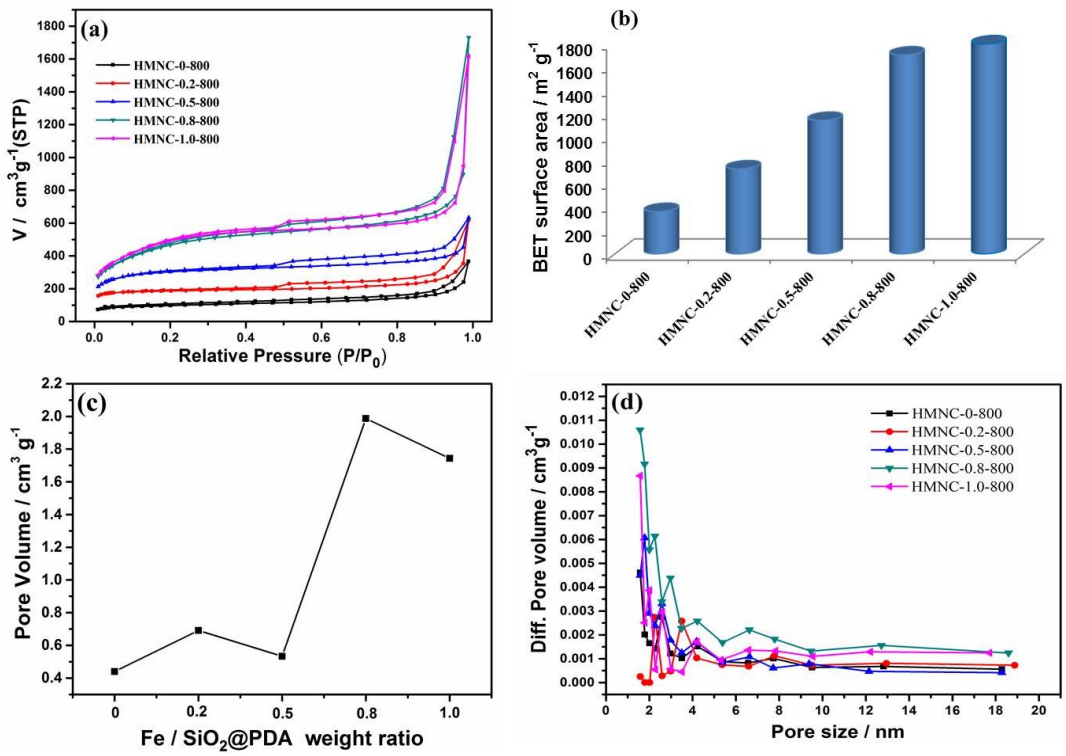

Figure S5. (a) Nitrogen adsorption and desorption isotherms of the HMNC catalysts annealed at 800 ℃. (b) The specific surface area of HMNC catalysts. (c) The corresponding pore size distribution curves calculated from the desorption branches. (d) The pore volume curves of HMNCs.

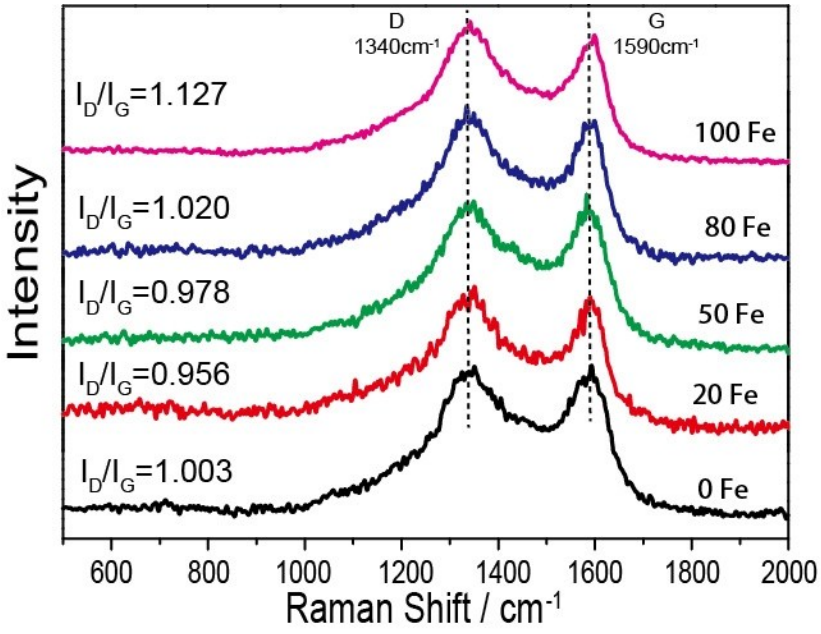

Figure S6. Raman spectrum of HMNC prepared at 800 ℃ with different Fe content

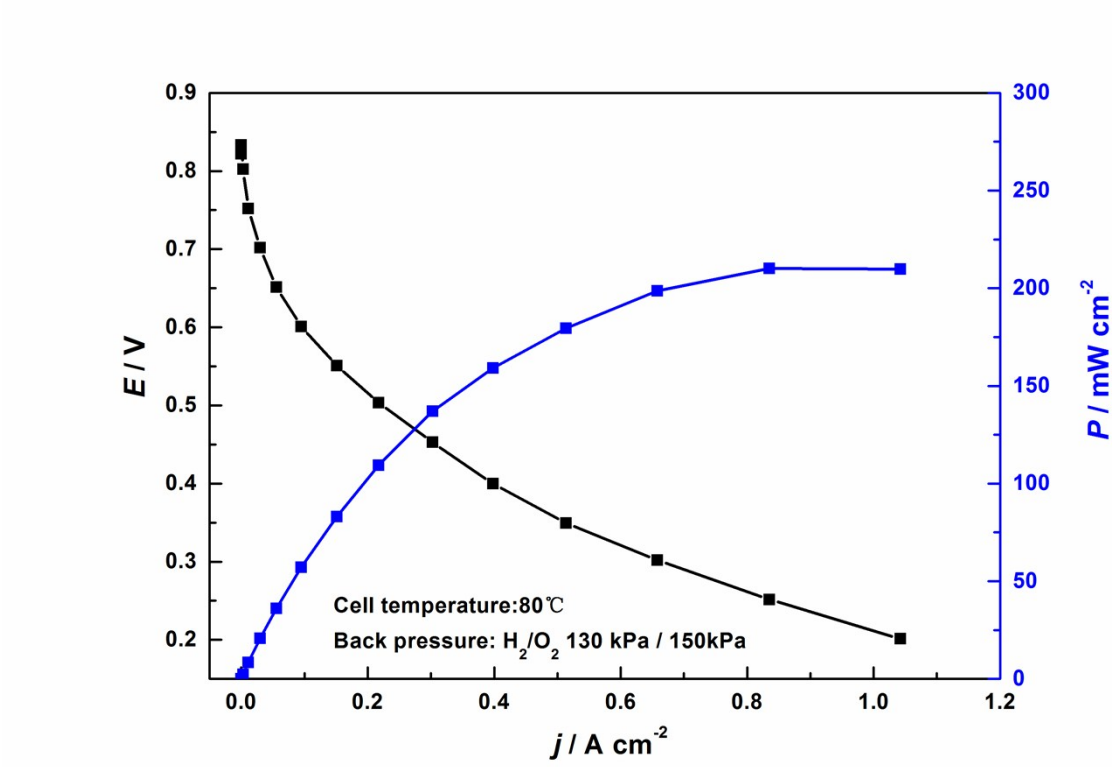

Figure S7. Polarization curves and corresponding power densities of membrane electrode assemblies fabricated with the HMNC-0.8-800 cathode catalyst whose loading was 3.0 mg cm^{-2}. The commercial Pt/C (20%) was used as anode; the Pt loading is 0.3 mg cm^{-2}.

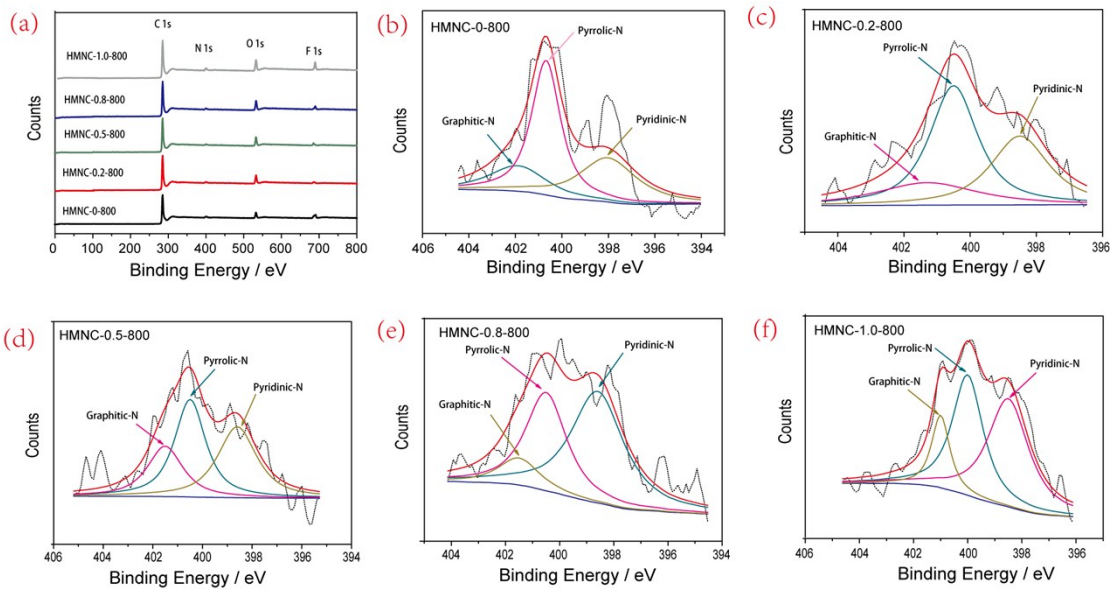

Figure S8. (a) XPS survey spectrum of HMNC prepared at 800 ℃ with different Fe content, XPS spectra of N 1s, (b) HMNC-0-800, (c) HMNC-0.2-800, (d) HMNC-0.5-800, (e) HMNC-0.8-800, (f) HMNC-0.5-800.

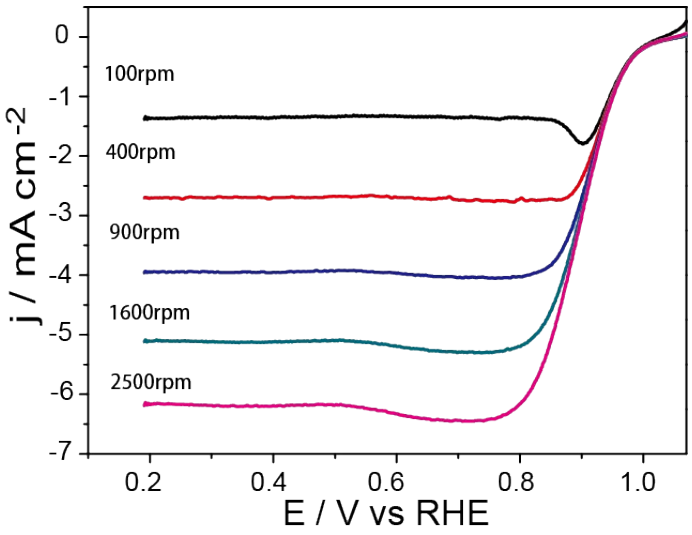

Figure S9. LSV curves of HMNC-0.8-800 in an O_2-saturated 0.1 M KOH at a sweep rate of 10 mV s^{-1} and different rotation rates.

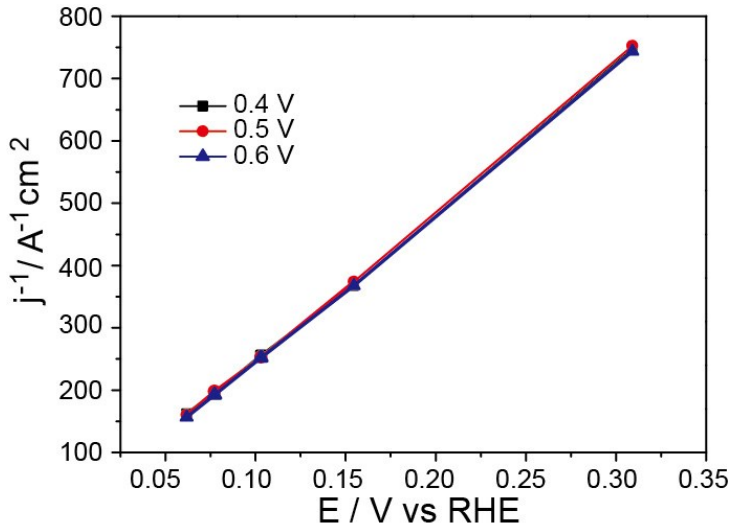

Figure S10. Koutecky–Levich plot of j^{-1} versus $\omega^{-1/2}$ at different electrode potentials.

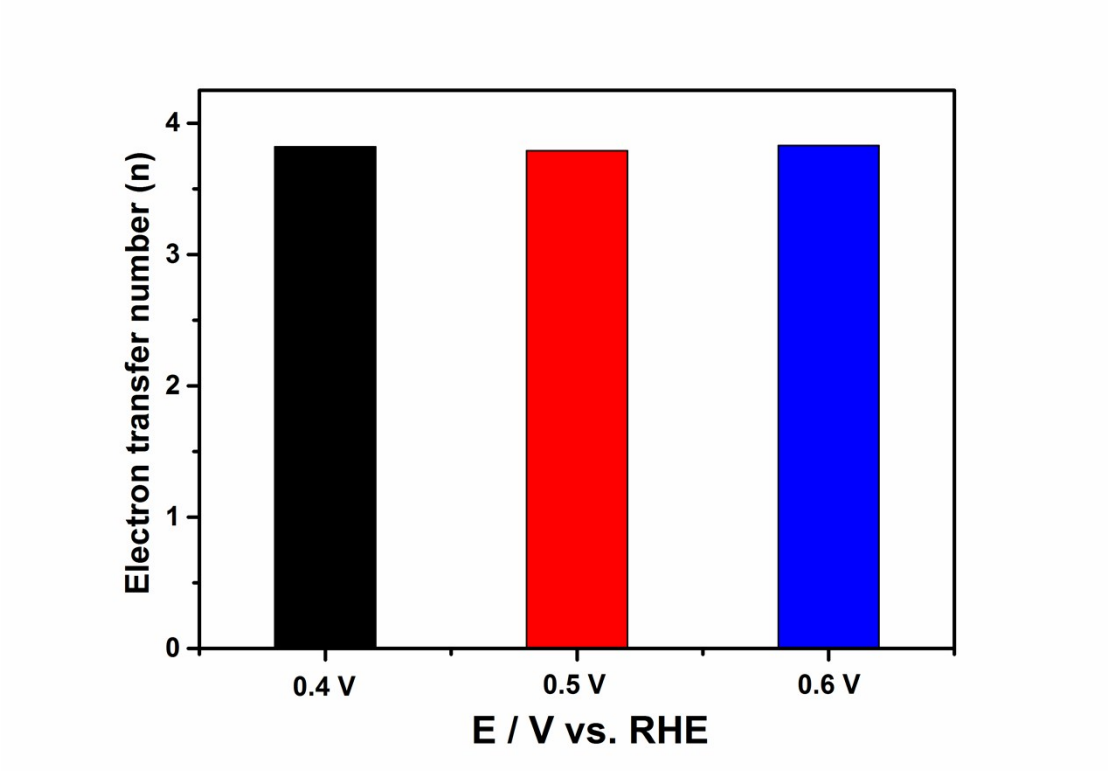

Figure S11. Electron transfer number of HMNC-0.8-800 at different potentials

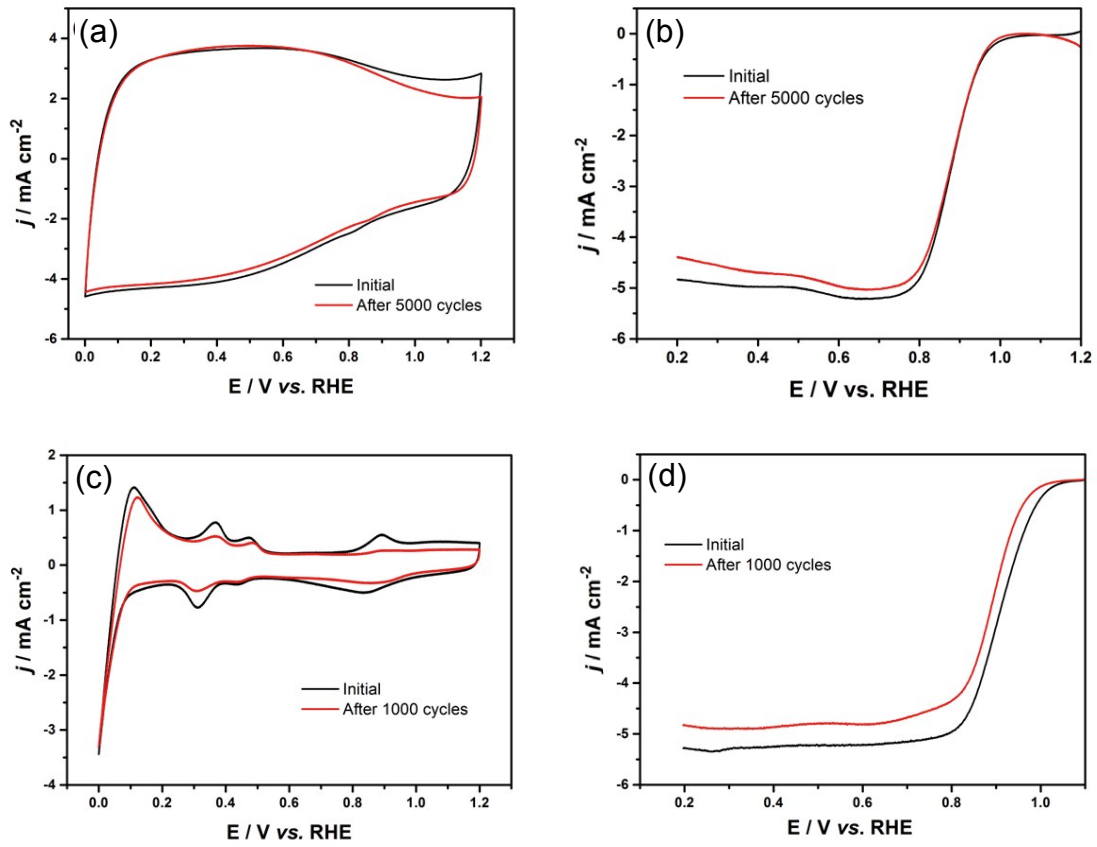

Figure S12. CV curves of (a) HMNC-0.8-800 and (c) commercial Pt/C catalysts before and after AST (recorded in N_2-saturated 0.1 M KOH with a sweep rate of 50 mVs^{-1}) , and ORR polarization curves on (b) HMNC-0.8-800 and (d) commercial Pt/C catalysts before and after AST (recorded in O_2-saturated 0.1 M KOH at 1,600 rpm and a scan rate of 10 $mV\ s^{-1}$).

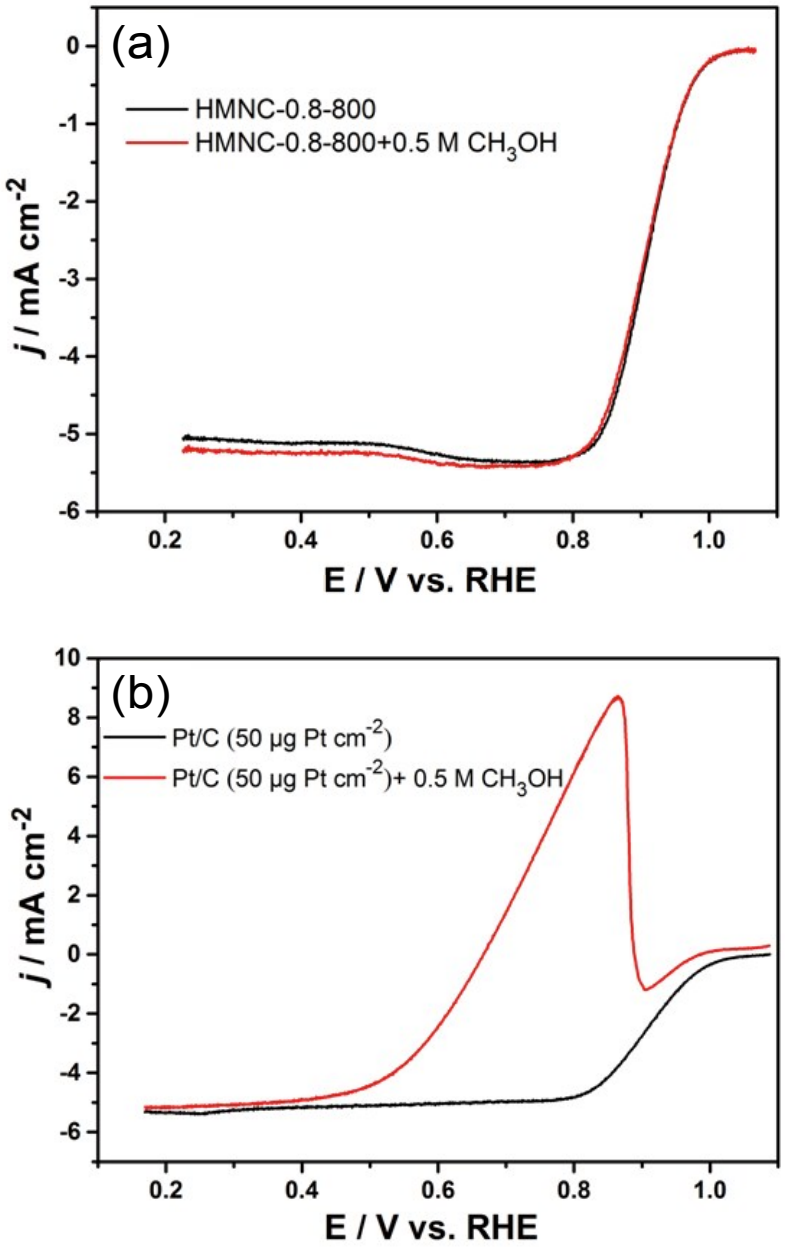

Figure S13. LSV curves of (a) HMNC-0.8-800 and (b) Pt/C catalyst in an O_2-saturated 0.1 M KOH, and in an O_2-saturated 0.1 M KOH upon the addition of 0.5 M CH_3OH at a sweep rate of 10 mV $s^{-1}$and 1,600 rpm rotating speed.

Table S1. Chemical compositions of HMNC samples obtained at different pyrolysis temperature estimated from XPS

Sample	C (at.%)	O (at.%)	Fe (at.%)	N (at.%)	Pyridinic-N (%)	Pyrrolic-N (%)	Quaternary-N (%)
HMNC-0.8-700	90.96	5.31	0.67	3.06	48.27	42.28	9.45
HMNC-0.8-800	87.88	9.86	0.14	2.12	53.53	36.42	10.05
HMNC-0.8-900	94.07	3.44	0.73	1.73	28.04	34.11	37.85

Table S2. BET surface areas, pore volume and average pore size calculated from adsorption and desorption isotherms for the HMNC catalysts

Samples	Surface area ($m^2 g^{-1}$)	Pore volume ($cm^3 g^{-1}$)	Average pore size (nm)
H-MNC-0-800	361.9	0.440	1.58
H-MNC-0.2-800	727.2	0.691	2.28
H-MNC-0.5-800	1142.7	0.533	1.78
H-MNC-0.8-800	1703.5	1.987	1.58
H-MNC-1.0-800	1797.4	1.744	1.58

Table S3. The onset potential, half-wave potential and diffusion-limiting current of the HMNC catalysts in Figure 3a.

Samples	Onset potential (V)	Half-wave potential $E_{1/2}$ (V)	J_D / 0.4V (mA cm^{-2})
HMNC-0-800	0.84	0.703	3.74
HMNC-0.2-800	0.94	0.774	3.96
HMNC-0.5-800	1.03	0.855	4.21
HMNC-0.8-800	1.06	0.911	5.12
HMNC-1.0-800	1.03	0.878	5.07
JM-Pt/C	1.06	0.898	5.21

Table S4. Summary of reported ORR performance of nitrogen-doped carbon catalysts. All catalysts were tested in 0.1 M KOH.

Catalyst	Catalyst loading (mg cm^{-2})	Half-wave potential (V)	Current density at 0.8 V (mA cm^{-2})	Reference
N-Doped Graphitic Carbon	0.1	0.78 V vs. RHE	2.30	2
Vertically ligned N-doped CNTs	unknown	0.84 V vs. RHE	2.65	3
Mesoporous N-Doped Carbons	0.079	0.82V vs. RHE	2.60	4
3D hierarchically porous NC	0.128	-0.133 V vs. Ag/AgCl	3.90	5
nitrogen-doped raphene/carbon nanotube nanocomposite	0.05	-0.32 V vs. Hg / Hg_2Cl_2	0.35	6
Phosphorus-doped g-C_3N_4	0.20	0.67 V vs. RHE	unknow	7
Ordered mesoporous C_3N_4/C	0.30	-0.23 V vs. Ag/AgCl	0.4	8
CNT/HDC(heteroatom-doped carbon)	0.6	0.82 V vs. RHE	3.50	9
Nitrogen-Doped Carbon Nanosheets	0.6	-0.13 V vs. Ag/AgCl	5.6	10
Hierarchically N-doped porous carbons	0.5	0.87 V vs. RHE	4.95	11
HMNC-0.8-800	**0.5**	**0.91V vs. RHE**	**5.3**	**This work**

Table S5. Summary of the fitting parameters obtained from Figure 3d.

Sample	R_Ω / Ω	R_{ct} / Ω	R_d / Ω
HMNC-0-800	53.28	286.6	—
HMNC-0.2-800	51.67	167.4	—
HMNC-0.5-800	55.26	114.9	12.05
HMNC-0.8-800	50.46	89.91	22.83
HMNC-1.0-800	50.44	112.6	13.81

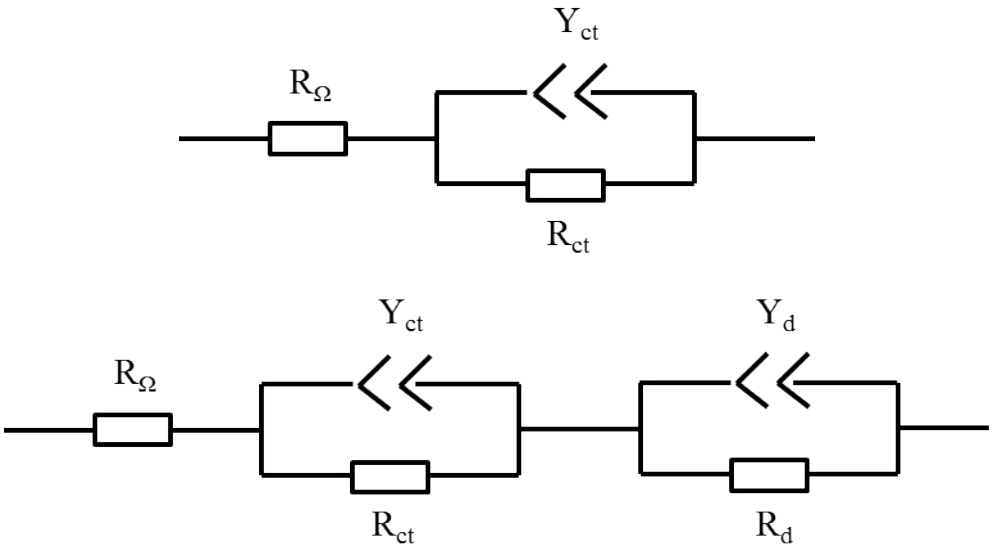

Table S6. Nitrogen contents calculated from XPS spectra

Samples	N (at%)	Pyridinic-N (%)	Pyrrolic-N (%)	Quatemary-N (%)
H-MNC-0-800	3.17	33.30	50.51	18.75
H-MNC-0.2-800	2.16	33.27	47.74	18.96
H-MNC-0.5-800	2.70	36.60	39.91	23.48
H-MNC-0.8-800	2.12	53.54	36.42	10.03
H-MNC-1.0-800	3.11[a]	46.75	39.31	13.94

[a] The higher content of Nitrogen was calculated by three times results. Unfortunately, underlying reasons are not clarified yet.

Reference:

1. W. Stöber, A. Fink and E. Bohn, J Colloid Interf Sci, 1968, **26**, 62-69.
2. Z. H. Xiang, D. P. Cao, L. Huang, J. L. Shui, M. Wang and L. M. Dai, Adv Mater, 2014, **26**, 3315-3320.
3. K. P. Gong, F. Du, Z. H. Xia, M. Durstock and L. M. Dai, Science, 2009, **323**, 760-764.
4. W. H. Niu, L. G. Li, X. J. Liu, N. Wang, J. Liu, W. J. Zhou, Z. H. Tang and S. W. Chen, J Am Chem Soc, 2015, **137**, 5555-5562.
5. W. H. He, C. H. Jiang, J. B. Wang and L. H. Lu, Angew Chem Int Edit, 2014, **53**, 9503-9507.
6. P. Chen, T. Y. Xiao, Y. H. Qian, S. S. Li and S. H. Yu, Adv Mater, 2013, **25**, 3192-3196.
7. T. Y. Ma, J. R. Ran, S. Dai, M. Jaroniec and S. Z. Qiao, Angew Chem Int Edit, 2015, **54**, 4646-4650.
8. Y. Zheng, Y. Jiao, J. Chen, J. Liu, J. Liang, A. Du, W. M. Zhang, Z. H. Zhu, S. C. Smith, M. Jaroniec, G. Q. Lu and S. Z. Qiao, J Am Chem Soc, 2011, **133**, 20116-20119.
9. Y. J. Sa, C. Park, H. Y. Jeong, S. H. Park, Z. Lee, K. T. Kim, G. G. Park and S. H. Joo, Angew Chem Int Edit, 2014, **53**, 4102-4106.
10. W. Wei, H. W. Liang, K. Parvez, X. D. Zhuang, X. L. Feng and K. Mullen, Angew Chem Int Edit, 2014, **53**, 1570-1574.
11. H. W. Liang, X. D. Zhuang, S. Brüller, X. L. Feng and K. Müllen, Nat Commun, 2014, **5**, 4973-4980.